Sayel M. Fayyad, Aiman Al Alawin,
Suleiman Abu-Ein, Zaid Abulghanam,
Abdel Salam Alsabag, Mohannad O. Rawashdeh,
Muntaser Momani, Waleed Momani

Aerodynamics Analysis Comparison between NACA 4412 and NREL S823 Airfoils

SAYEL M. FAYYAD*, AIMAN AL ALAWIN, SULEIMAN ABU-EIN,
ZAID ABULGHANAM, ABDEL SALAM ALSABAG, MOHANNAD O. RAWASHDEH,
MUNTASER MOMANI, WALEED MOMANI
Department of Mechanical Engineering, Faculty of Engineering Technology,
Al-Balqa Applied University,
Amman,
JORDAN

*Corresponding Author

Abstract: - This paper presents a study of the aerodynamics of a wing or bluff bodies and compares different wing types' behavior against aerodynamic forces. NACA 4412 and NERL S823 airfoils will be analyzed numerically using the ANSYS simulation. The methodology used in this paper depends on collecting data from the last studies, studying the analyzed airfoil models, and constructing an analytical model to show the aerodynamic effects on NACA 4412 and NERL S823 airfoils, and find the total solution. A comparison between NACA 4412 airfoil and NREL'S S823 is presented. It was found that the lift coefficient for NACA 4412 values is higher than that of NREL S823 airfoil but for NACA 4412 such values are decreasing as the angle of attack (AoA) is increasing till $8°$ of AoA after that Cl values are increasing slightly. In contrast, for NREL S823 airfoil the values of lift coefficient (Cl) are increasing with AoA till $8°$ after that they become constant or slightly decreasing, while for drag coefficient, it can be noticed that values of drag coefficient (Cd) for NACA 4412 are lower than that of NREL S823 airfoils and for all values of angle of attack, also values for both airfoils are decreasing with AoA till $8°$ and then slightly increased.

1 Introduction

Aerodynamics is the science of how a body travels through the air. As a result, it is a branch of dynamics concerned with the motion of air and other gases, as well as the forces acting on a moving or stationary object in an air current. As a result, there are three main components to flight aerodynamics. Examples of these components are airplanes, relative winds, and the atmosphere.

An airfoil is a surface that is designed to elicit a certain reaction from the air it passes through. As a result, an airfoil is any component of an aircraft that transforms air resistance into a force useful for flight. A propeller's blades are so engineered that as they revolve, their form and location generate a stronger pressure to build up behind them than in front of them so that they pull the airplane forward.

The objective of this study is to numerically evaluate several types of airfoils (wings or bluff bodies) with varied parameters using ANSYS and then compare the results to determine the ideal conditions for airfoil designs, including geometry. Two types of airfoils are being studied: NACA 4412 and NREL airfoils. The major goal of this work, as described above, is to examine the NACA 4412 and NREL's airfoils using the ANSYS simulation and compare the findings with varied airfoil geometry and aerodynamic circumstances. Any airfoil contains top and lower surfaces. The essential point is the higher density of streamlines above the wing, even though the top surface of the average wing profile is curvier than the lower surface. The larger the density of streamlines, the faster the air flows. According to Bernoulli's principle, a rise in fluid speed happens at the same time as a decrease in pressure or potential energy. This is identical to the energy conservation principle. The total of all kinds of mechanical energy in a fluid along a streamline is the same at all places along that streamline in a steady flow, [1].

Because of the effect of the wing planform, airfoil section properties differ from wing or aircraft

Sayel M. Fayyad, Aiman Al Alawin,
Suleiman Abu-Ein, Zaid Abulghanam,
Abdel Salam Alsabag, Mohannad O. Rawashdeh,
Muntaser Momani, Waleed Momani

properties. From root to tip, a wing can have varied airfoil sections with taper, twist, and sweepback. The action of each part along the span determines the wing's resulting aerodynamic qualities, [1]. The lift over drag (L/D) ratio is often used to determine a wing's efficiency. This ratio changes depending on the angle of attack, but it always reaches a maximum value for a specific angle of attack. The wing has reached its optimum efficiency at this angle. The shape of the airfoil is the factor that defines the most efficient angle of attack for the wing, as well as the degree of efficiency. The maximum thickness of the most efficient airfoils for common usage is found roughly one-third of the way back from the leading edge of the wing, according to research, [1]. High-lift wings and high-lift devices for wings have been developed by shaping the airfoils to produce the desired effect. The amount of lift produced by an airfoil will increase with an increase in the wing chamber. An increase in the wing chamber will enhance the amount of lift produced by an airfoil. The curvature of an airfoil above and below the chord line surface is referred to as a camber. The upper chamber denotes the upper surface, the lower camber denotes the lower surface, and the mean camber denotes the section's mean line. Camber is positive when the chord line departs inward, and negative when it departs outward. As a result, the upper surface of high-lift wings has a considerable positive camber and the lower surface has a slight negative camber. By enlarging the upper chamber and producing a negative lower chamber, wing flaps allow a regular wing to approximate this state [1].

It's also known that the bigger the wingspan is in comparison to the chord, the more lift is obtained. Aspect ratio is the term for this comparison. The greater the lift, the higher the aspect ratio. Despite the advantages of increasing the aspect ratio, structural and drag factors were determined to be significant limits. The total amount of drag on an aircraft is made up of many drag forces with three main: Parasite drag; Profile drag and Induced drag.

Parasite drag is the result of a complex interaction of many drag forces. Any exposed thing aboard an aircraft creates air resistance, and the more objects in the airstream, the parasite drag will be greater. While parasite drag can be decreased by decreasing the number of exposed parts to a minimum and simplifying their design, the sort of parasite drag that is the most difficult to reduce is skin friction. There is no such thing as a perfectly smooth surface. When inspected under magnification, even machined surfaces have a ragged, uneven appearance. The air near the surface is deflected by these jagged surfaces, creating resistance to smooth circulation. By adopting glossy flat finishes and removing protruding rivet heads, roughness, and other abnormalities, skin friction can be decreased.

NACA 4412 and NREL's airfoils

The NACA four-digit wing sections define the profile as follows:

1. One digit describing the maximum camber as a percentage of the chord

2. One digit describing the distance of maximum camber from the airfoil leading edge in tens of percent of the chord

3. Two digits describing the maximum thickness of the airfoil as a percent of the chord, [2].

From 1984 to 1993, the NREL S823 designed and developed seven families of airfoils, each with 23 variants suitable for different rotor diameters. The NREL S823 airfoil (Figure 1) was chosen from among the 23 airfoil variants based on the availability of experimental data, [3] and [4]. The NERL S823 was compared to another designated airfoil DU 06-W-200 which was considered to be laminar and unsymmetrical and designed for vertical axis wind turbine at Delft University of Technology in the year 2006 (Figure 1), [5].
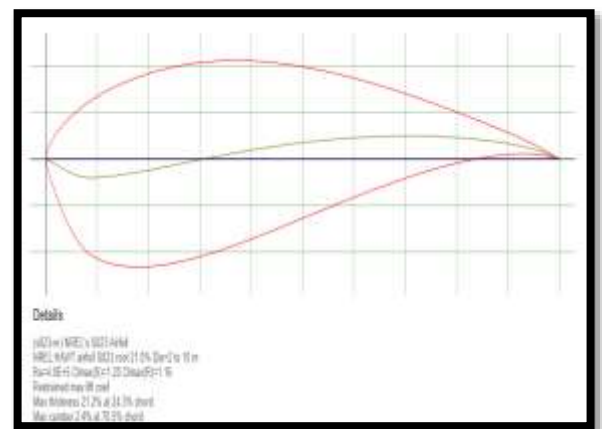

Fig. 1: NREL's S823- (ONERA OA213 AIRFOIL - NERA/Aerospatiale OA213 rotorcraft)

Many studies have been conducted on this critical issue. The application of Computational Fluid Dynamics (CFD) in the simulation and design of high subsonic transport aircraft wings. RAMPANT, an unstructured, multigrid flow solver, was used to perform the computation. CATIA was used to create a 2-D and 3-D modeling of the wing. The grid of the wing was created by using TGrid and preBFC software. The paper describes the grid creation technique as well as the application of CFD to the wing design process. It then goes over the advantages and disadvantages of using the

Sayel M. Fayyad, Aiman Al Alawin,
Suleiman Abu-Ein, Zaid Abulghanam,
Abdel Salam Alsabag, Mohannad O. Rawashdeh,
Muntaser Momani, Waleed Momani

aforementioned tools. The wing is then optimized using the results of the aerodynamic analysis. It concludes with a discussion of the findings and suggestions future for research, [6]. The authors in [7], addressed the issue of ionic flapping aircraft gliding performance by numerical simulation method implementing two-way fluid-structure interaction (FSI), the investigation included the angle of attack, a rigid and flexible wing, the elastic model effects and velocity on the aerodynamic features of a gliding aircraft, at an angle of attack of 10°, minor effect on the aerodynamic performance of the aircraft was observed, holding maximum lift to drag ratio for both the flexible and rigid wings]. It was also found that with an increase in the gliding speed, the lift force increased while the lift can't support the gliding movement at low speed. To achieve gliding, the weight of the micro air vehicle is kept under control at around 3 g with the gliding speed assured to be more than 6.5 m/s. The findings of this study have significant implications for the design of bionic flapping aircraft. The authors in [8], discussed the most prominent applications of morphing concepts for both two and three-dimensional wing models. Various methods and tools usually used for the design and analysis of these concepts, ranging from aerodynamic to structural analyses, and from control to optimization aspects, are discussed. During the review process, it became clear that the acceptance of morphing concepts for routine use on aerial vehicles is still limited, and some reasons for this are given. Lastly, promising future applications are identified. Designing the blade for low wind power density regions was discussed in [9]. Wind turbine blade aerodynamic airfoils have a significant impact on wind turbine aerodynamic efficiency. This entails selecting an appropriate airfoil section for the proposed wind turbine blade. In their study, NACA 4412 airfoil profile was used to analyze wind turbine blades. GAMBIT 2.4.6 is used to create the airfoil geometry. CFD analysis is performed using FLUENT 6.3.26 at various angles of attack ranging from 0° to 120°. The coefficients of lift and drag are calculated for a Reynolds number of 1x105. A comparative study of various airfoils from the NACA and NREL Airfoil families is presented in [10], with a focus on their suitability for small wind turbines. Four comparison criteria have been considered in this case. Maximum glide ratio at lower and higher Reynolds numbers, angle of attack difference between lower and higher Reynolds numbers, and percentage deviation of maximum glide ratio from stall point are the criteria. XFOIL analysis using Q-blade software yields the data

required for comparing two families of airfoils, revealing that NACA airfoils have better average performance criteria while NREL airfoils have better stability criteria. The authors in [11], determined aerodynamic coefficients for different wing spans with various ground clearances, it was found that short-span wings have the tendency to delay the beginning of separation and eventually lose negative lift. Due to vortices, there wasn't a significant change in the strength or size at the wing end plate, these vortices, at short-span wings, affected a larger percentage of the wing encouraging the flow to stay attached and mitigate the opposite pressure gradient which will lead to separation at longer spans, as a result, it was demonstrated that shorter span wings have lower lift coefficient as compared to larger span wings. A reviewing for flapping wing aerodynamics modeling, including wing kinematics and the Navier-Stokes equation is presented in [12]. Also reviewed was the mathematical formulation of normal forces, chord-wise forces, total forces, lift, and thrust. It has recently been demonstrated that a flexible wing is far superior to a rigid wing. The authors in [13], investigated many flapping wing aerodynamics topics numerically and experimentally. These topics cover some of the most recent advances in flapping wing aerodynamics, such as wake structure analysis, the effects of airfoil thickness and kinematics on aerodynamic performance, vortex structure analysis around 3D flapping wings, and kinematics optimization. Both experimental and numerical approaches are used to investigate the wake structures behind a sinusoidal pitching NACA0012 airfoil. The experiments are carried out using Particle Image Velocimetry (PIV), and two types of wake transition processes are distinguished, namely the transition from a drag-indicative wake to a thrust-indicative wake and the transition from a symmetric wake to an asymmetric wake. The developed SD solver's numerical results agree well with the experimental results. The initial conditions, such as the initial phase angle, are found numerically to determine the deflective direction of the asymmetric wake. The [14] is focused on estimating the performance of a small wind turbine blade with a suitable dimple arrangement at 25% and the middle of the chord length for NREL S228 and S238, the conducted CFD analysis used k-ε turbulence model by ANSYS Fluent software by which the aerodynamic performance and the moment equations are solved, a delay flow separation was observed at the dimple entrance leading to creation of vortices, the investigation also includes a simulation for the blade with an adequate

Sayel M. Fayyad, Aiman Al Alawin,
Suleiman Abu-Ein, Zaid Abulghanam,
Abdel Salam Alsabag, Mohannad O. Rawashdeh,
Muntaser Momani, Waleed Momani

overall performance by the help of GH BLADED and the obtained results are discussed. According to [15], an effort was made by simulating the selected airfoils using Q Blade open-source software at the National Renewable Energy Laboratory (NREL), namely S823 and DU 06-W-200. Q Blade software employs a special algorithm called the double multiple stream tube (DMS) for the assessment of horizontal axis wind turbines (VAWTs) and the blade element method (BEM) for assessing horizontal axis wind turbines (HAWTs). The graphical user interface (GUI) of Q Blade includes the viscous-in-viscid coupled panel process code XFOIL for calculating the lift and drag coefficients of an airfoil at any angle of attack (AoA). The simulation is performed and compared at various Reynolds numbers ranging from 1x105 to 3x105 for both selected airfoils. For each applied Reynolds number, results show that the S823 airfoil with a higher lift coefficient up to 10° AoA, than the DU 06-W-200 airfoil has higher values, the pattern is true for the lift-to-drag ratio. Lastly, the simulation results are validated by comparing them to the obtained experimental data, which shows good agreement between the Q Blade simulation result and those for experimental data. According to the NACA four-digit wing sections, in which the profile is defined as follows: one digit describes maximum camber distance from the airfoil leading edge in tens of percent of the chord; one digit describes maximum camber as a percentage of the chord; and then two digits describing the maximum thickness of each airfoil as a percentage of the chord, [16].

When a stream of air flows over and under an airfoil in motion, it produces a total aerodynamic force. The point of impact is when the air splits and flows around the airfoil. The point of collision creates a high-pressure region or stagnation point. The high-pressure region is often positioned near the lower section of the leading edge, depending on the angle of attack. This high-pressure region adds to the overall force produced by the blade. The entire aerodynamic force, also known as the resultant force, may be separated into two components: lift and drag. Lift acts on the airfoil perpendicular to the relative wind. Drag is the resistance or force that resists the airfoil's motion through the air. It operates on the air.foil in a direction that is parallel to the relative wind. Many factors influence the overall lift produced by an airfoil. Increased speed creates lift by creating a bigger pressure difference between the top and lower surfaces. Lift fluctuates with the square of the speed, rather than increasing in direct proportion to it, [17].

2 Problem Formulation

2.1 CFD Analysis of NACA 4412 and NREL's S823 Airfoils

First of all, NACA 4412 airfoil coordinates file was imported into ANSYS Design Modeler, and then a C-type boundary was created around it for meshing, CFD analysis, and post-processing results. A pressure-based solver with a steady-state solution was used in conjunction with the Spalart-Allmaras viscous model. The fluid is air entering the domain at a rate of 18 m/s, and the outlet boundary condition is pressure-based. FLUENT generates a residual for each governing equation that is solved, and the residual indicates how well the present solution meets the governing equation's discrete form. The solution is iterated in this instance until the residual for each equation is less than 1e-6. The working pressure is 101.325 kPa, the turbulent viscosity ratio is 10%, the airfoil chord length is 1m, the pressure-velocity coupling scheme is SIMPLE, and Second-Order Upwind is utilized to calculate pressure and momentum. Figure 2 shows the NACA 4412 airfoil and its mesh, [18], [19], [20].
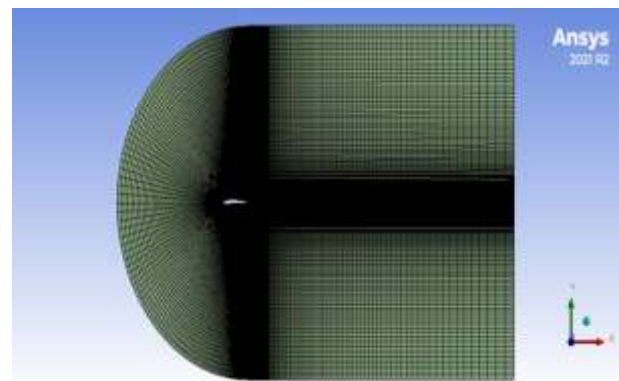

Fig. 2: The meshing used for NACA 4412

The study employed a steady-state, pressure-based solver, and finite volume discretization to solve the k-epsilon model's governing equations. Designers monitored the numerical solution error to make sure it was converging properly. A 5 m radial and 10 m long C-type computational domain was selected. During simulations, air (density = 1.225 kg/m3 and dynamic viscosity = 1.7894 e-05 Pa s) is employed as a fluid flow medium. This was accomplished by using grids of varying sizes to establish a mesh independence study. This was done by raising the number of grid elements until the solution demonstrated little change with additional increases in the mesh density. The residuals of the governing differential equation's outcome variable are used to assess the convergence speed throughout

Sayel M. Fayyad, Aiman Al Alawin,
Suleiman Abu-Ein, Zaid Abulghanam,
Abdel Salam Alsabag, Mohannad O. Rawashdeh,
Muntaser Momani, Waleed Momani

the iteration phase. Additionally, for each of the incorporated force coefficients, the relative differences between two sequential iterations are used to verify convergence. Double precision, 2D analysis was conducted using normal k-epsilon flow equations, and a continuous flow of air was seen around the plane's perimeter. The lift force is determined by the spacecraft's weight, whereas the drag force is determined by the airplane's aerodynamic efficiency and its wingspan. Table 1 shows boundary conditions applied on these airfoils.

Table 1. Boundary conditions applied

Air density	1.225 kg/m3
Viscosity	1.7894e-05 kg/m-s
Inlet velocity	18 m/s
Wall Motion	Stationary Wall
Shear Condition	No Slip
Outlet Gauge Pressure	0 Pa
Pressure-Velocity Scheme	Coupled
Pressure, Momentum, Turbulent kinetic energy & dissipation rate	Second-order upwind
Gradient	Least Square Cell-Based

3 Results and Discussion

3.1 NACA 4412 Airfoil Results

The findings indicate an area of high pressure at the leading edge (stagnation point) of the airfoil and a low-pressure zone on the top airfoil surface. The Bernoulli equation states that pressure and velocity are inversely linked; thus, velocity will be lower in high-pressure areas. The pressure applied to the bottom surface of the airfoil was higher than the pressure applied to the entering flow stream, and therefore, the airfoil was simply forced upward, perpendicular to the arriving flowing fluid. Figure 3 shows the Drag coefficient of NACA 4412 Airfoil results.
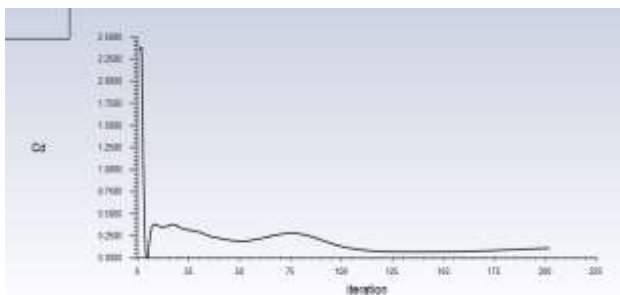

Fig. 3: Drag coefficient graph

Figure 4 shows the lift coefficient as a function with a number of iterations of analysis.
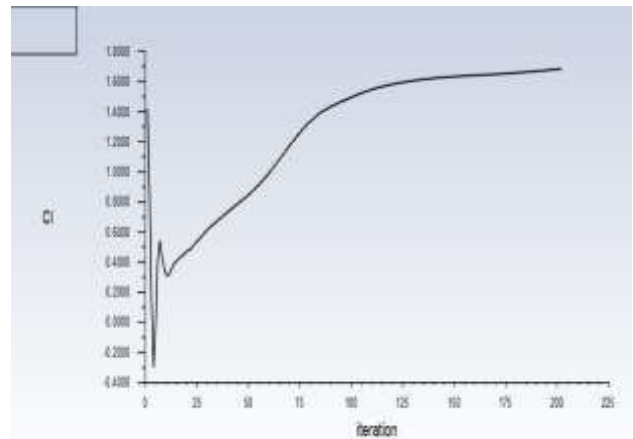

Fig. 4: Lift coefficient graph

Figure 5 shows the pressure coefficient as a function of position (m) on the airfoil.
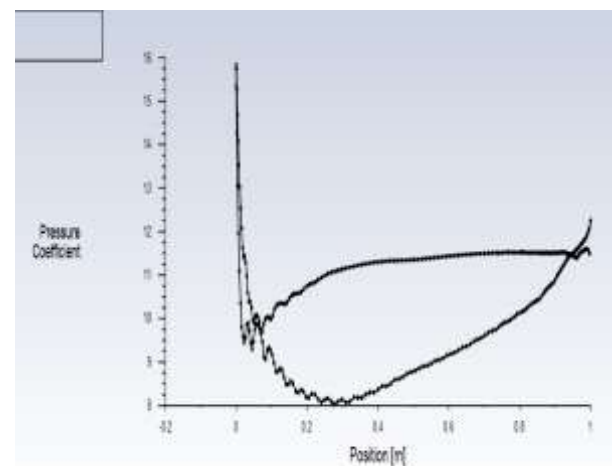

Fig. 5: Pressure coefficient chart

Figure 5 depicts a pressure coefficient chart; the pressure distribution of NACA airfoil profiles is estimated using the numerical panel technique for 2D lifting air flow circumstances. The fluctuation in pressure coefficients along the chord is seen by analyzing the airfoil shape exposed to various AOA (angle of attack) conditions, including stalling angles. The zero lift AOA of the profiles is also examined to determine the impact of thickness-to-chord ratios on airfoil properties. Figure 6 shows the velocity contours of the NACA 4412 airfoil, it can be noticed that red areas have maximum velocity values while blue-colored areas have the minimum values of velocity.

Sayel M. Fayyad, Aiman Al Alawin,
Suleiman Abu-Ein, Zaid Abulghanam,
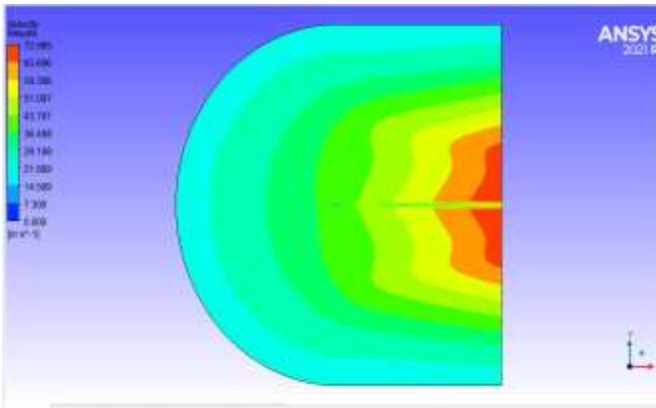Abdel Salam Alsabag, Mohannad O. Rawashdeh,
Muntaser Momani, Waleed Momani

Fig. 6: Velocity contours

Figure 7 shows the pressure contours of the NACA 4412 airfoil, it can be noticed that red areas have maximum pressure values while blue-colored areas have the minimum values of pressure.
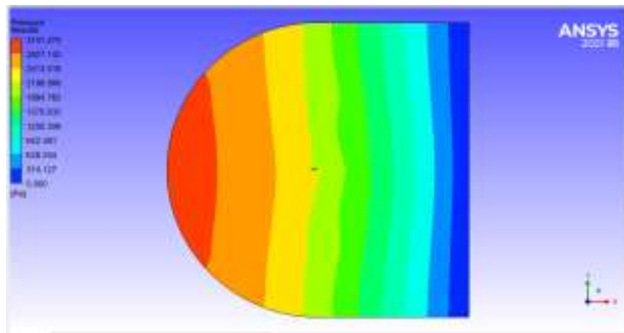

Fig. 7: Pressure contours

Figure 8 shows the pressure values at 0° attack angle the maximum value of pressure at the tip of the airfoil with 3141.270 Pa, while the minimum pressure is 1570 Pa at the top of the airfoil.
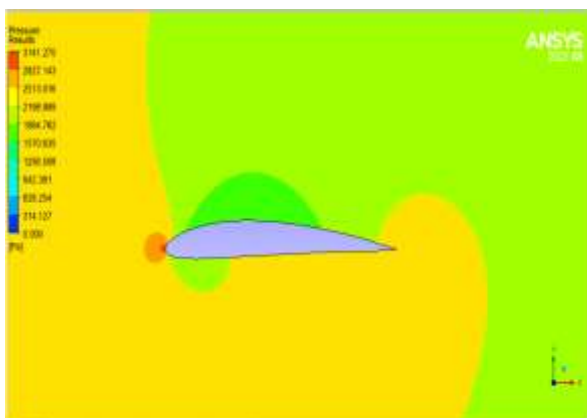
Fig. 8: Pressure contours for 0° AoA

Figure 9 shows the velocity values at 0° attack angle it is clear that the maximum value of velocity at the top (upper surface) of the airfoil with 55 m/s, while the minimum velocity is from 14-21 m/s at the front and lower surface of the airfoil.
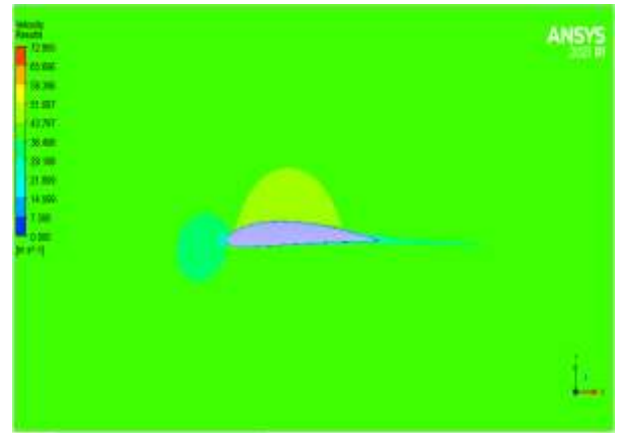
Fig. 9: Velocity contours for 0 deg. AoA

Figure 10 shows the pressure values at a 2° attack angle it is clear that the maximum values of pressure at the tip (front) of the airfoil with 155.252-191.962 Pa, while the minimum pressure is -138.428 Pa at the top (upper surface) of the airfoil
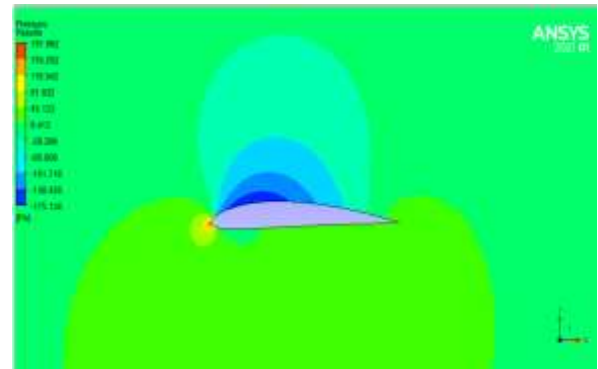

Fig. 10: Pressure contours for 2 deg. AoA

Figure 11 shows the velocity values at 2° attack angle it is clear that the maximum values of velocity at the top (upper surface) of the airfoil with 22.013-24.459 m/s, while the minimum velocity is from 2.446-7.338 m/s at the front and lower surface of the airfoil.
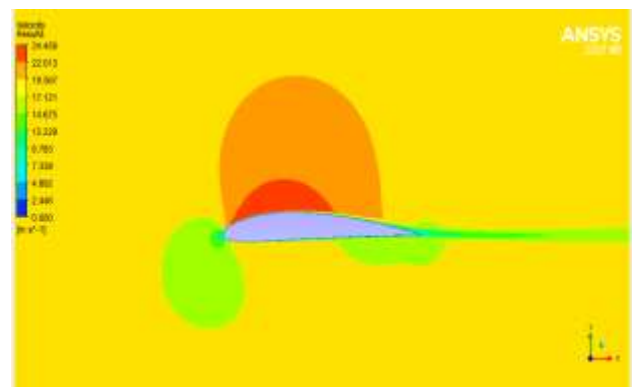

Fig. 11: Velocity contours for 2° AoA

Sayel M. Fayyad, Aiman Al Alawin,
Suleiman Abu-Ein, Zaid Abulghanam,
Abdel Salam Alsabag, Mohannad O. Rawashdeh,
Muntaser Momani, Waleed Momani

Figure 12, Figure 13, Figure 14, Figure 15, Figure 16 and Figure 17 show values of pressure and velocity at different values of attack angle (6, 8, and 12 degrees) respectively.
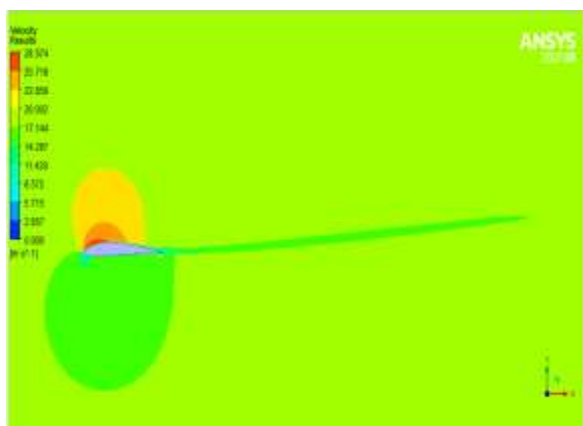

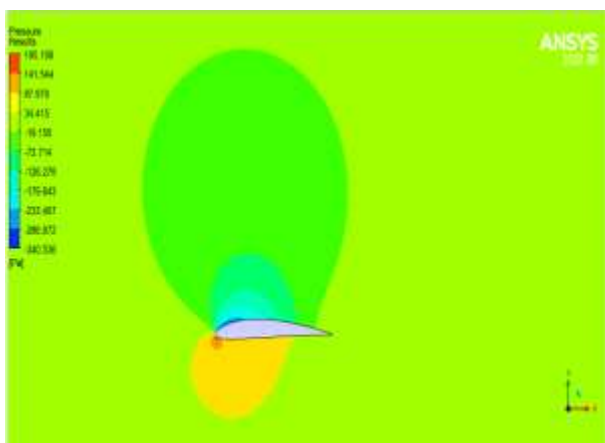Fig. 12: Velocity contours for 6° AoA

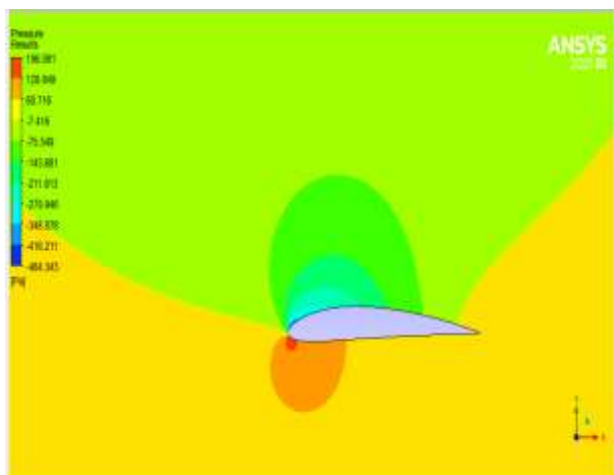Fig.13: Pressure contours for 6° AoA

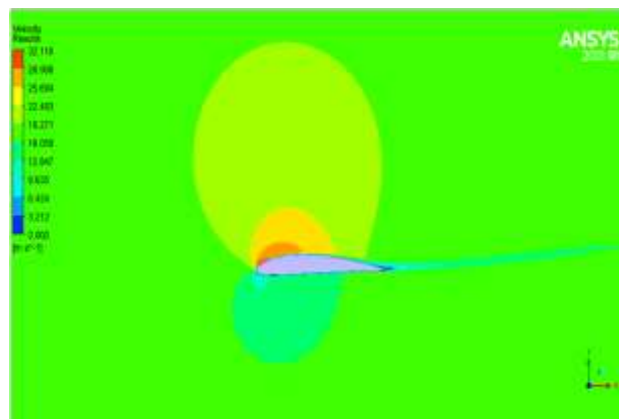Fig. 14: Pressure contours for 8° AoA
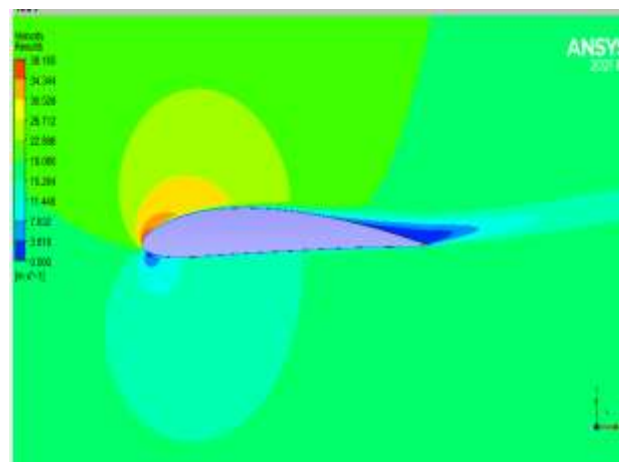

Fig. 15: Velocity contours for 8° AoA

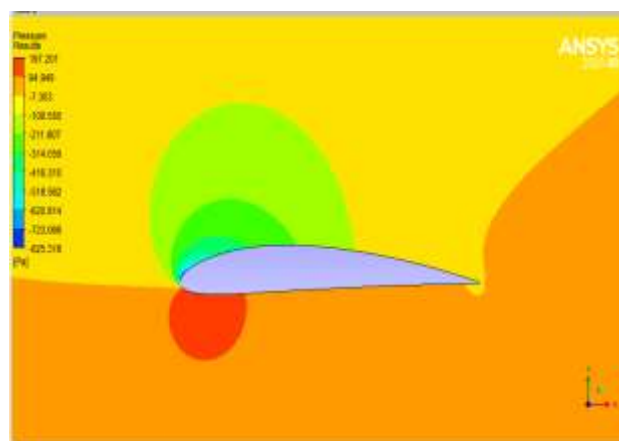Fig. 16: Velocity contours for 12° AoA

Fig. 17: Pressure contours for 12° AoA

Table 2 shows the Final results of Cd and Cl for NACA 4412.

Table 2. Results of Cd and Cl for NACA 4412

Angle of Attack	Lift coefficient (Cl)	Drag coefficient (Cd)
0	1.683	0.11
2	0.567	0.0137
6	0.943	0.0175
8	1.113	0.021
12	1.3376	0.04

Sayel M. Fayyad, Aiman Al Alawin,
Suleiman Abu-Ein, Zaid Abulghanam,
Abdel Salam Alsabag, Mohannad O. Rawashdeh,
Muntaser Momani, Waleed Momani

A linear relation was observed between the angle of attack (AoA) and Lift/Drag ratio up to 8° AoA which means the Cd/Cl ratio increases with increasing angle of attack up to 8°. On the contrary, after 8^0 it showed an inverse relation, and the Lift/Drag ratio started decreasing with increasing AoA value.

3.2 NREL's S823 Airfoil

The airfoil families developed by the National Renewable Energy Laboratory (NREL) are generally resistant to relative roughness effects, resulting in somewhat reduced yearly energy losses. Additionally, the airfoils are usually modified to have a thicker body, resulting in unexpected performance characteristics. The use of blade tip airfoils with a low Glade ratio and a scoop that correlates with the control of the maximum power may result in further performance improvement while operating a stall-regulated turbine. This allows 100 percent to fifteen tons of sweptback rotor area for a given generator size, depending on the design. The S-Series airfoils from NREL are available in both thin and thick families. The thin airfoil families are well suited for stalling controlled wind turbines in situations where performance losses due to airfoil change of state are critical considerations. The change in the state of the airfoil is not a significant disadvantage for variable pitch and variable speed turbines. In most cases, the main airfoil is used in conjunction with root and tip airfoils. Most turbine blades are made up of a circular portion that connects to the hub. NREL airfoil curves are somewhat smoother and have a distinctive form, even if the flow conditions change while concerns with noise and discontinuity in power production for stall-controlled wind turbines may arise on airfoils with camber ridges on specific NACA airfoils. Figure 18 shows the lift coefficient of NREL'Ss823 Airfoil results with the number of iterations.
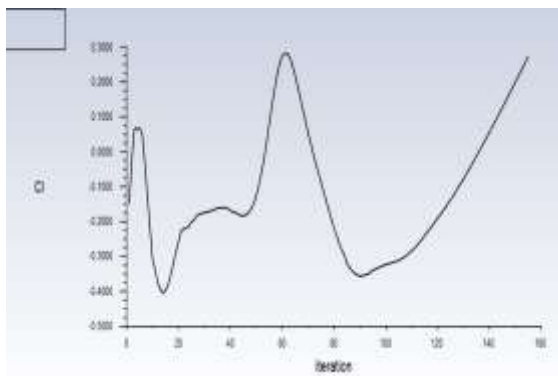

Fig. 18: Lift coefficient graph for NREL's S823

Figure 19 shows the drag coefficient as a function with the number of iterations of the analysis.
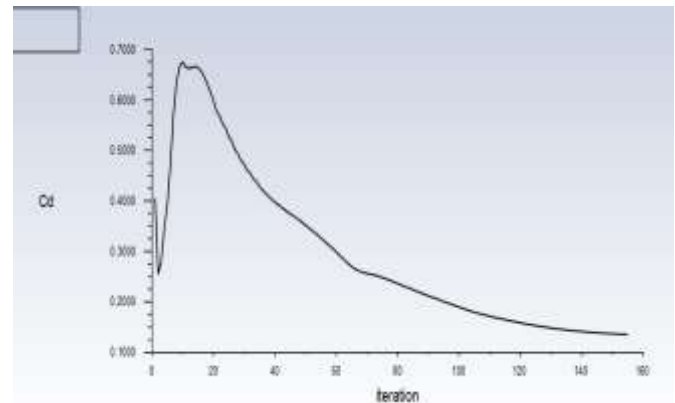

Fig. 19: Drag coefficient graph for NREL's S823

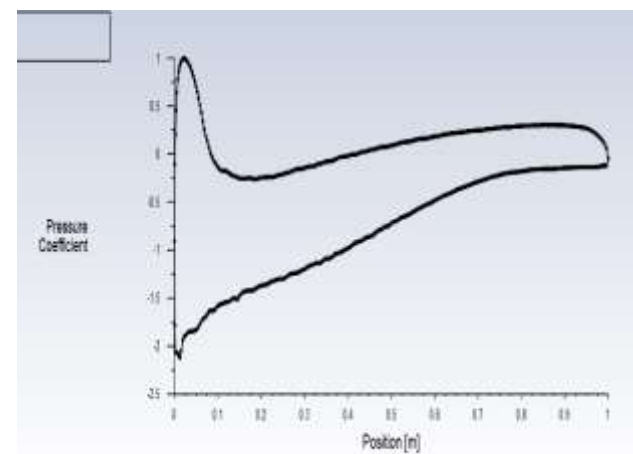Figure 20 shows the pressure coefficient as a function of position (m) on the airfoil

Fig. 20: Pressure coefficient chart

Figure 21 shows the pressure contours of NREL's S823 airfoil, it can be noticed that red areas have maximum pressure values (3044.380 Pa) while blue-colored areas has the minimum values of pressure (608.876).

Sayel M. Fayyad, Aiman Al Alawin,
Suleiman Abu-Ein, Zaid Abulghanam,
Abdel Salam Alsabag, Mohannad O. Rawashdeh,
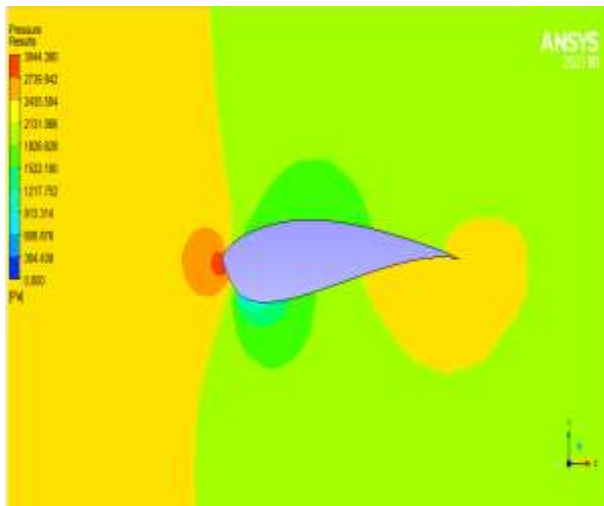Muntaser Momani, Waleed Momani

Fig. 21: Pressure contours for NREL's S823 (AoA = 0 deg.)

Figure 22 shows the velocity contours of NREL's S823 airfoil, it can be noticed that red areas have maximum velocity values (71.782 m/s) while blue-colored areas have the minimum values of velocity (7.178 m/s).
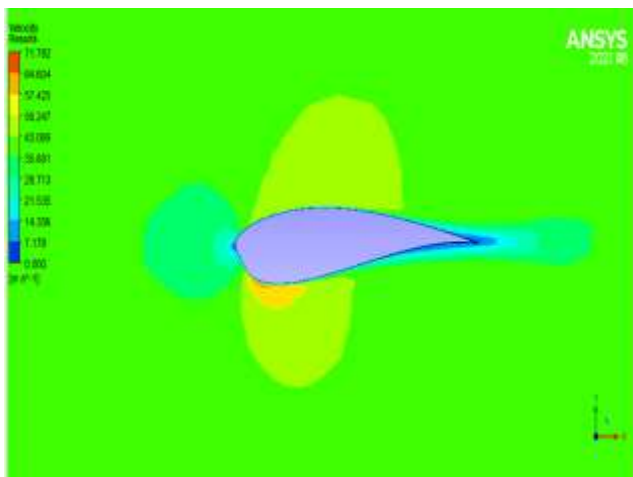

Fig. 22: Velocity contours for NREL's S823 (AoA = 0 deg.)

Figure 23, Figure 24, Figure 25 and Figure 26 show the velocity and pressure distribution values at 8 and 12 attack angles respectively for NREL's S823 airfoil.
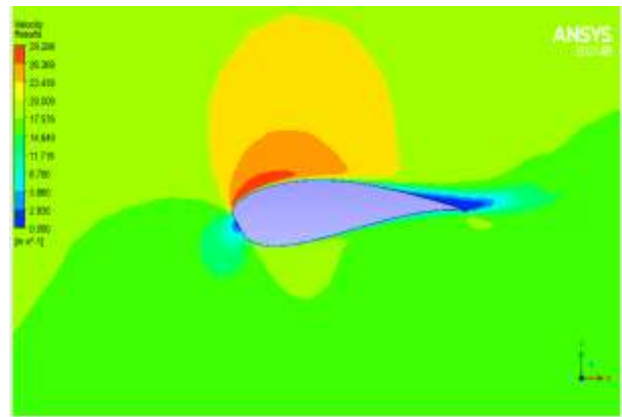

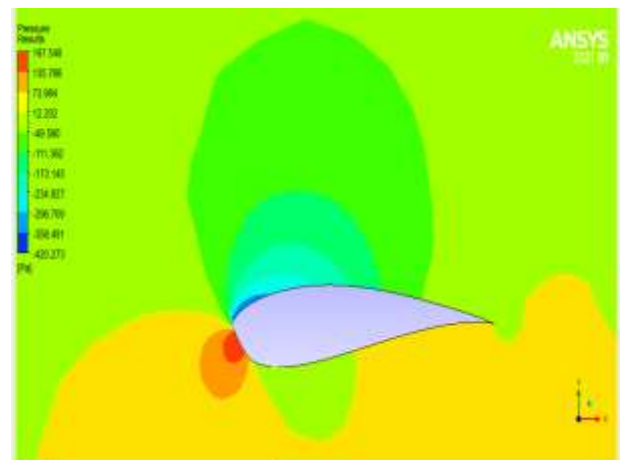Fig. 23: Velocity contours for NREL's S823 (AoA = 8 deg.)

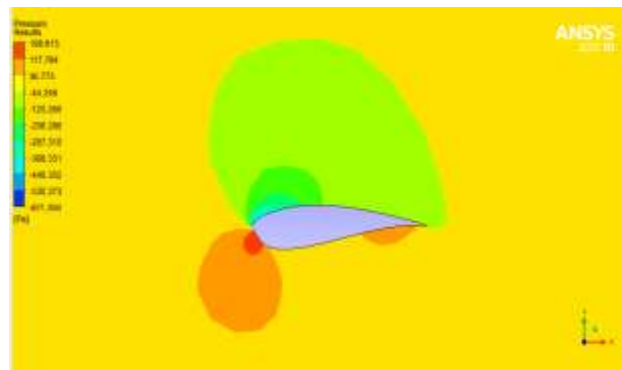Fig. 24: Pressure contours for NREL's S823 (AoA = 8 deg)

Fig. 25: Pressure contours for NREL's S823 (AoA = 12 deg)

Sayel M. Fayyad, Aiman Al Alawin,
Suleiman Abu-Ein, Zaid Abulghanam,
Abdel Salam Alsabag, Mohannad O. Rawashdeh,
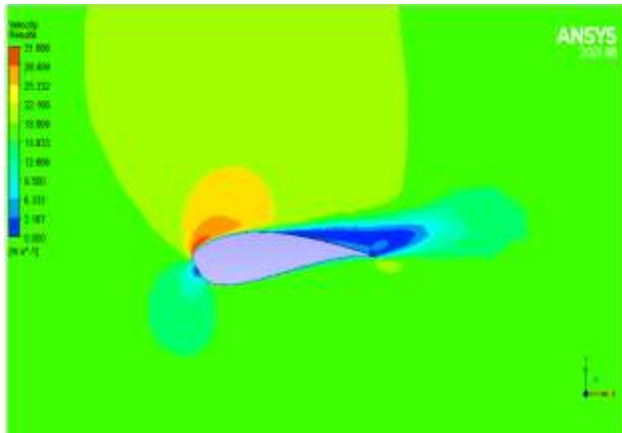Muntaser Momani, Waleed Momani

Fig. 26: Velocity contours for NREL's S823 (AoA = 12 deg)

It can be noticed that for NREL's S823 airfoil, there are no values determined at attack angles of 2 and 6 degrees. To compare the results of the targeted airfoils at 1232877 Reynolds number and the vast range of blade angles of attack from 0 to 12 degrees, the airflow simulations provided lift coefficient and drag coefficients. The governing equation was solved, and the flow issue was addressed using the usual k-epsilon model, coupled algorithm, and second-order upwind approach provided in this study. The k-epsilon model with better wall treatment is the most suited CFD model due to its low error. The k-epsilon (k−ϵ) model for turbulence is commonly used to simulate mean flow characteristics for turbulent flow situations. It is an Eddy viscosity model, which is a type of turbulence model used to determine Reynolds stress. This is a two-equation model. That is, in addition to the conservation equations, it solves two transport equations (PDEs) to account for historical effects such as convection and turbulent energy diffusion. Two variables are transported: turbulent kinetic energy (k), which determines the energy in turbulence, and turbulent dissipation rate (ϵ), which defines the rate of dissipation of turbulent kinetic energy, [21].

3.3 Comparison of the Two Airfoils
One objective of this study is to compare the values of both lift and drag coefficient values for both airfoils under study: NACA 4412 and NERL S823 airfoils at different attack angles, Table 3 shows a comparison value of Drag coefficient and lift coefficients at 0, 8, and 12 degrees of attack angles.

Table 3. CFD results comparison

Angle of Attack	NACA 4412		NREL's S823	
	Lift coefficient (Cl)	Drag coefficient (Cd)	Lift coefficient (Cl)	Drag coefficient (Cd)
0	1.683	0.11	0.273	0.1355
8	1.113	0.021	0.9258	0.041
12	1.3376	0.04	0.983	0.094

Figure 27 shows a comparison between the Drag coefficient values of the two airfoils NACA 4412 and NREL's S823 airfoils.

From Table 3 and Figure 27, it can be noticed that NACA 4412 airfoil has a more lift coefficient values than that of NERL S823, while the NERL S823 airfoil has more Drag coefficient values than that of NACA 4412 airfoil at all attack angles this is because of the airfoil shape and dimensions.

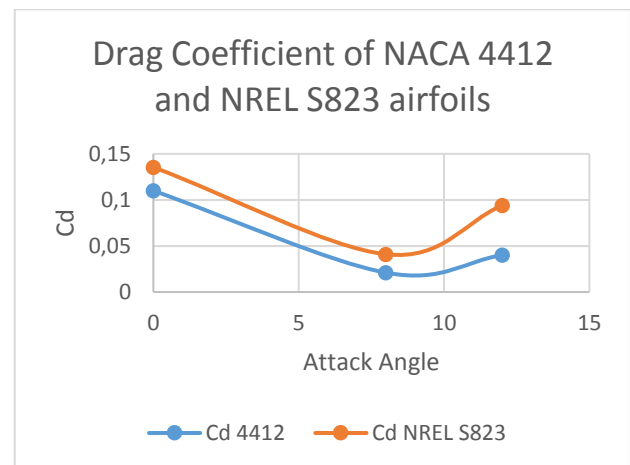Fig. 27: Drag Coefficient of the two airfoils NACA 4412 and NREL S823

It can be noticed that values of Cd of NACA 4412 are lower than that of NREL S823 airfoils for all values of angle of attack, also values for the two airfoils are decreasing with AoA till 8 degrees and then increase slightly. Figure 28 shows a comparison between Lift coefficient values of the two airfoils NACA 4412 and NREL's S823 airfoils.

Sayel M. Fayyad, Aiman Al Alawin,
Suleiman Abu-Ein, Zaid Abulghanam,
Abdel Salam Alsabag, Mohannad O. Rawashdeh,
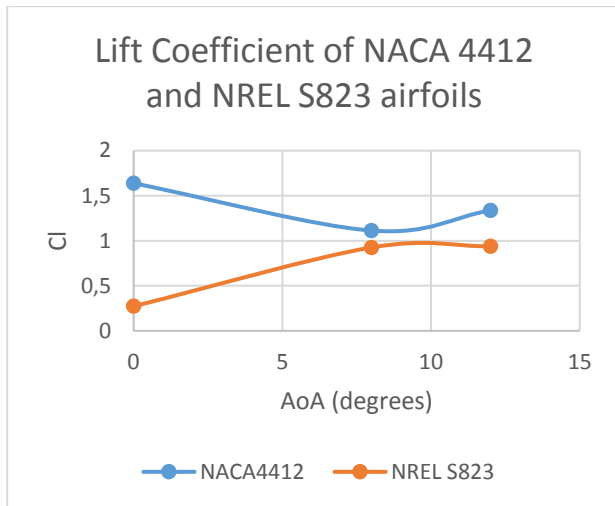Muntaser Momani, Waleed Momani

Fig. 28: Lift Coefficient of NACA 4412 and NREL S823 airfoils

It can be noticed that the lift coefficient for NACA 4412 values is higher than that of NREL S823 airfoil but for NACA 4412 such values are decreasing as AoA is increasing till 8 degrees of AoA after that Cl values are increasing slightly. In contrast, for NREL S823 airfoil the values of Cl are increasing with AoA till 8 ° after that they become constant or decrease slightly.

From Table 4 the momentum exerted on the two types of airfoils can be calculated using the following equations

-For drag force (D)

$$D= (0.5)*Cd*A*\rho*V^2 \qquad (1)$$

Where Cd is the drag coefficient, A: is the reference area, and ρ: is air density. And so, the momentum is

$$MD=D*S \qquad (2)$$

Where S is the distance (position from the tip of the airfoil), the Lift force is given as:

$$L= Cl(A*0.5*\rho*V^2) \qquad (3)$$

So, the momentum resulting from lift force is given as:

$$ML=L*S \qquad (4)$$

Using data from Table 3, the momentum resulted from both drag and lift of the two wings (at 0, 8, and 12 AoA) as follows (assume ρ=1.4 kg/m3, v is taken at average value, approximate area A=0.1 m^2 (24 inches x 6 inches) for both). See Table 4 and Table 5 for results.

Table 4. Drag and lift forces and momentum calculations for NACA 4412 airfoil

NACA 4412						
Angle of Attack	Lift coefficient (Cl)	Drag coefficient (Cd)	Lift force N.	ML N.m (at mid-span x=0.3 m)	Drag force(N)	MD
0	1.683	0.11	152.682	45.80	9.98	3.00
8	1.113	0.021	19.95	5.98	0.376	0.11
12	1.3376	0.04	33.80	10.140	1.011	0.303

Table 5. Drag and lift forces and momentum calculations for NREL S823 airfoil

NREL's S823						
Angle of Attack	Lift coefficient (Cl)	Drag coefficient (Cd)	Drag force(N)	MD (N. m)	Lift force (N)	ML (N. m)
0	0.273	0.1355	12.22	3.66	24.77	7.43
8	0.9258	0.041	0.646	0.20	14.5782	4.373
12	0.983	0.094	1.685	0.505	17.615	5.284

3.4 Discussion

It can be noticed that the drag coefficient for both airfoils decrease as AoA increases to 9 degrees, after this angle and for both airfoils it starts to increase. Also, the CD for NACA 4412 is lower than NERL S823 for 12 degrees (AoA). The lift coefficient of NACA 4412 is higher than that of NERL S823 for all angles of attack, CD for both airfoils are decreasing as AoA increases to 9 degrees, then it increases slightly till 12 degrees for NACA 4412 and slightly constant to decrease for NERL S823 airfoil.

4 Conclusion

In the performance criterion, NACA airfoils have shown superior results, while in the stability criteria, things are opposite. Generally, ANSYS Fluent is suitable for aerodynamic analysis of wind turbine blades, results show that a turbulent layer produces more significant drag at lower airfoil angles of attack. In designing wind turbine blades, it is critical to ensure that the airfoil utilized does not develop any instabilities in operation. Special care is required if using a pitch-controlled wind turbine. Stabilizing the angle of attack is very important to maintain proper operability. When looking at many technical requirements that wind turbines must satisfy, it is clear that one will have to choose

Sayel M. Fayyad, Aiman Al Alawin,
Suleiman Abu-Ein, Zaid Abulghanam,
Abdel Salam Alsabag, Mohannad O. Rawashdeh,
Muntaser Momani, Waleed Momani

between several airfoils. These provide the functions of crucial aerodynamic, mechanical, reusability, and supportability requirements. Aspects such as electromagnetic interference, acoustic noise production, and aesthetic appearance are generally expected to be less critical for alternate rotor features. Traditionally, in aircraft lifting surface theory, people assume a positive relationship between high lift and low drag and that the lift-to-drag ratio may be a significant concept. This art of the debate is different from aircraft wing airfoils. For the first issue, rotor performance reveals that the product of the chord and the lift coefficient must be greater than one. Operational at a better lift constant will enable the use of smaller blades. When it comes to vicious power losses, the overall viscous torsion is determined by the L/D ratio of the airfoil, which limits the vicious power losses, but the specific amount of lift does not dictate viscous torsion itself. The drag coefficient for both airfoils decreases as AoA increases until 9 degrees, at which point it begins to increase for both airfoils. Furthermore, for 12 degrees, NACA 4412 has a lower CD than NERL S823 (AoA). For all angles of attack, the lift coefficient of NACA 4412 is greater than that of NERL S823. CD for both airfoils decreases as AoA increases until 9 degrees, then increases slightly until 12 degrees for NACA 4412 and remains slightly constant to decrease for NERL S823 airfoil

References:

[1] KSU, *Basic Aerodynamics*. Category B1/B2 according to Part-66 Appendix 1-KSU, Issue 1, 2017, pp: 1-74.

[2] Chandrala M., Abhishek Choubey, "Bharat Gupta Aerodynamic Analysis of Horizontal Axis Wind Turbine Blade", *IJERA*, Vol. 2, Issue 6, 2012.

[3] Tangler JL, Somers DM (1995) NREL Airfoil families for HAWTs; January 1995 NREL fTP-442–7109, [Online]. https://www.nrel.gov/docs/legosti/old/7109.pdf (Accessed Date: December 25, 2023).

[4] Anyoji, M., and Hamada, D. (2019). High-performance Airfoil with low Reynolds-number Dependence on aerodynamic characteristics. *Fluid Mechanics Research International Journal.* 2019; 3(2):76–80.

[5] Claessens MC (2006). *The design and testing of Airfoil for application in small vertical axis wind turbines*, Master of Science Thesis, Faculty of Aerospace Engineering, Delft University of Technology, 9th Nov 2006.

[6] Edi P. (2014). The Simulation and Design of High Subsonic Wing Aircraft. *Proceeding of the 1st International Conference on Computer Science and Engineering 2014*.

[7] Wang C., Yu Ning, Xinjie Wang, Junqiu Zhang, and Liangwen Wang (2020). Simulation Analysis of the Aerodynamic Performance of a Bionic Aircraft with Foldable Beetle Wings in Gliding Flight. *Applied Bionics and Biomechanics* Vol. 2020, Article ID 8843360, 12 pages.

[8] Li D., Zhao, S., Ronch, A., Xiang, J., Drofelnikb, J., Lia, Y., Lu Zhang, Wu, Y., Kintscher, M., Monner, H., Rudenko, A., Guo, S., Yin, W., Kirn, J., Stefan Storm, S., and Breuker, R. (2018). A Review of Modelling and Analysis of Morphing Wings. *Progress in Aerospace Sciences*, Vol. 100, Issue June 2018, pp. 46-62.

[9] Kevadiya M., Hemish A. Vaidya (2013). 2D Analysis of NACA 4412 Airfoil. International *Journal of Innovative Research in Science, Engineering and Technology*. Vol. 2, Issue 5.

[10] Islam R., Labid Bin Bashar, Dip Kumar Saha, Nazmus Sowad Rafi (2019). Comparison and Selection of Airfoils for Small Wind Turbine between NACA and NREL's S series Airfoil Families. *International Journal of Research in Electrical, Electronics and Communication Engineering*. Vol. 4, Issue 2.

[11] Diasinos S., Tracie J Barber, and Graham Doig (2012). Influence of wingspan on the aerodynamics of wings in ground effect. Proc IMechE Part G: J *Aerospace Engineering,* 10(3) 1–5.

[12] Chalia S., Manish Kumar Bharti (2016). A Review on Aerodynamics of Flapping Wings. *International Research Journal of Engineering and Technology (IRJET)*. Vol. 3, Issue 3.

[13] Yu M. (2012). *Numerical and experimental investigations on unsteady aerodynamics of flapping wings*. A dissertation of Doctor of Philosophy in Aerospace Engineering-Iowa State University.

[14] Robin K. (2019). Design and Analysis of Dimple Arrangement on a Small Wind Turbine Blade. *International Journal of Innovative Technology and Exploring Engineering (IJITEE),* Vol. 9, Issue 2.

[15] Reddy K., Bachu Deb, and Bidesh Roy (2021). Analysis of the Aerodynamic Characteristics of NREL S823 and DU 06-W-200 Airfoils at Various Reynolds Numbers Using Q-blade. *Emerging Trends in*

WSEAS TRANSACTIONS on FLUID MECHANICS
DOI: 10.37394/232013.2024.19.13

Sayel M. Fayyad, Aiman Al Alawin,
Suleiman Abu-Ein, Zaid Abulghanam,
Abdel Salam Alsabag, Mohannad O. Rawashdeh,
Muntaser Momani, Waleed Momani

Mechanical Engineering, Lecture Notes in Mechanical Engineering, Springer, Singapore. https://doi.org/10.1007/978-981-15-8304-9_20.

[16] *Impact Energy Method for Establishing the Design Standards for UAV Systems*, Appendix to JAA/ Euro-control UAV Task-Force Final Report, Enclosure 3, and May 2004.

[17] Sadrehaghighi, I. (2023). *Aerodynamics of Airfoils and Wings (including Case Studies)*. Technical Report, June 2023, DOI: 10.13140/RG.2.2.12882.63682/1.

[18] Kandwal S., and S. Singh, "Computational Fluid Dynamics Study of Fluid Flow and Aerodynamic Forces on an Airfoil," *IJERT*, Vol. 1, Issue 7, September 2012.

[19] Logsdon N., "*A procedure for numerically analysing Airfoil and Wing sections,*" The Faculty of the Department of Mechanical & Aerospace Engineering University of Missouri – Columbia, 2006.

[20] Tangler, J. L., & Somers, D. M. (1995). *NREL Airfoil families for HAWTs* (No. NREL/TP-442-7109). National Renewable Energy Lab., Golden, CO (United States).

[21] Chakraborty, N. (2021). Turbulence Modelling of Air Flow around an Aerofoil. *Experiment Findings* · May 2021. DOI: 10.13140/RG.2.2.25981.49125.

Contribution of Individual Authors to the Creation of a Scientific Article (Ghostwriting Policy)
- Sayel M. Fayyad carried out the simulation
- Aiman Al Alawin: editing and writing
- Suleiman Abu-Ein: literature review
- Zaid Abulghanam: writing and figures
- Abdel Salam Alsabag: writing discussion
- Mohannad O. Rawashdeh: writing conclusion
- Muntaser Momani: Literature review.
- Waleed Momani: Methodology

Conflict of Interest
The authors have no conflicts of interest to declare.